

RESEARCH

Open Access



# Splenic proteome profiling in response to Marek's disease virus strain GX0101 infection

Chuan Wang<sup>1\*</sup>, Yuanzi Liu<sup>2</sup>, Yuze Yang<sup>3</sup>, Man Teng<sup>4</sup>, Xuerui Wan<sup>1</sup>, Zixiang Wu<sup>1</sup> and Zhao Zhang<sup>1\*</sup>

## Abstract

Marek's disease virus (MDV) strain GX0101 was the first reported field strain of recombinant gallid herpesvirus type 2 (GaHV-2). However, the splenic proteome of MDV-infected chickens remains unclear. In this study, a total of 28 1-day-old SPF chickens were intraperitoneally injected with chicken embryo fibroblast (CEF) containing 2000 PFU GX0101. Additionally, a control group, consisting of four one-day-old SPF chickens, received intraperitoneal equal doses of CEF. Blood and various tissue samples were collected at different intervals (7, 14, 21, 30, 45, 60, and 90 days post-infection; dpi) for histopathological, real-time PCR, and label-free quantitative analyses. The results showed that the serum expressions of MDV-related genes, *meq* and *gB*, peaked at 45 dpi. The heart, liver, and spleen were dissected at 30 and 45 dpi, and their hematoxylin-eosin staining indicated that virus infection compromised the normal organizational structure at 45 dpi. Particularly, the spleen structure was severely damaged, and the lymphocytes in the white medulla were significantly reduced. Furthermore, liquid chromatography-mass spectrometry (LC-MS) and label-free techniques were used to analyze the difference in splenic proteome profiles of the experimental and control groups at 30 and 45 dpi. Proteomic analysis identified 1660 and 1244 differentially expressed proteins (DEPs) at 30 and 40 dpi, respectively, compared with the uninfected spleen tissues. According to GO analysis, these DEPs were involved in processes such as organelle organization, cellular component biogenesis, cellular component assembly, anion binding, small molecule binding, metal ion binding, cation binding, cytosol, nuclear part, etc. Additionally, KEGG analysis indicated that the following pathways were linked to MDV-induced inflammation, apoptosis, and tumor: Wnt, Hippo, AMPK, cAMP, Notch, TGF- $\beta$ , PI3K-Akt, Rap1, Ras, Calcium, NF- $\kappa$ B, PPAR, cGMP-PKG, Apoptosis, VEGF, mTOR, FoxO, TNF, JAK-STAT, MAPK, Prion disease, T cell receptor, and B cell receptor. We finally screened 674 DEPs that were linked to MDV infection in spleen tissue. This study improves our understanding of the MDV response mechanism in the spleen.

**Keywords** Marek's disease, GX0101, Chicken, Proteomics, Label-free technique

## Introduction

Marek's Disease (MD), a serious threat to chicken health, causes huge economic losses to the poultry industry worldwide [1, 2]. It is an immunosuppressive malignant tumor disease, characterized by increased T lymphocytes, and is caused by the infection of MDV in chickens [3]. The MD leads to diverse physiological dysfunctions in chickens, typically including the following five: 1) immunosuppression and lymphoma formation in the lymphatic system; 2) atherosclerotic injury of the cardiovascular system; 3) various

\*Correspondence:

Chuan Wang  
wangchuan@gsau.edu.cn  
Zhao Zhang  
zzhao0829@163.com

<sup>1</sup> College of Veterinary Medicine, Gansu Agricultural University, Lanzhou 730070, PR China

<sup>2</sup> Shaanxi Meili-OH Animal Health Co., Ltd, Xi'an 712034, PR China

<sup>3</sup> Beijing Animal Husbandry Station, Beijing 100107, PR China

<sup>4</sup> Key Laboratory of Animal Immunology of the Ministry of Agriculture, Henan Provincial Key Laboratory of Animal Immunology, Henan Academy of Agricultural Sciences, Zhengzhou 450002, PR China



© The Author(s) 2023. **Open Access** This article is licensed under a Creative Commons Attribution 4.0 International License, which permits use, sharing, adaptation, distribution and reproduction in any medium or format, as long as you give appropriate credit to the original author(s) and the source, provide a link to the Creative Commons licence, and indicate if changes were made. The images or other third party material in this article are included in the article's Creative Commons licence, unless indicated otherwise in a credit line to the material. If material is not included in the article's Creative Commons licence and your intended use is not permitted by statutory regulation or exceeds the permitted use, you will need to obtain permission directly from the copyright holder. To view a copy of this licence, visit <http://creativecommons.org/licenses/by/4.0/>. The Creative Commons Public Domain Dedication waiver (<http://creativecommons.org/publicdomain/zero/1.0/>) applies to the data made available in this article, unless otherwise stated in a credit line to the data.

peripheral and central nervous system lesions; 4) formation of sporadic or diffuse tumors of different sizes in the viscera with destruction of normal tissue structure; and 5) epithelium injury and the formation of skin feather sac knots. MDV infection induces tumors and immune organ atrophy in the host, resulting in immune suppression [4, 5].

The natural infection process of MDV has four major stages: early cytolitic infection, latent infection, late cytolitic infection, and transformational infection [6]. *Meq* and *gB* (glycoprotein B) are the two MDV-related genes; *meq* directly participates in the development of MD tumors, while *gB* is the most conserved structural gene of MDV. *gB* encodes a group of glycoprotein complexes containing eight glycosylation sites [7]. *gB* is located on the surface of the infected cell membrane and cytoplasm, promoting humoral and cellular immunity in the host, and therefore it is the main neutralizing antigen of MDV. *gB* proteins mainly participate in virus adsorption and invasion into host cells [8].

Past research has studied the host protein expression at different stages of MDV infection in chicken immune organs by two-dimensional electrophoresis (2-DE) and mass spectrometry (MS). For example, chickens were infected with the MDV RB1B strain in the bursa of Fabricius and spleen to examine transcriptome change post-infection [9, 10]. Another study examined the splenic proteome of chickens infected with the MDV JM-16 strain [11]. MDV Chinese strain GX0101 was isolated in 2001 from a vaccinated flock of layer chickens with severe tumors. It was the first reported field strain of recombinant gallid herpesvirus type 2 (GaHV-2) [12]. Reticuloendotheliosis virus (REV) long terminal repeat (LTR) insert promoted horizontal transmission of MDV strain GX0101 compared to other viral strains [13, 14]. GX0101 is a very virulent MDV (vvMDV) with higher horizontal transmission ability than the other vvMDV strain, Md5. The complete genome sequence of GX0101 is 178,101 nucleotides [15]. The *meq* deletion mutant of GX0101 showed significantly reduced immunosuppression in chickens [16]. Although the changes in the splenic transcriptome of GX0101-infected chickens during early infection and pathogenic phases have been determined by RNA-seq [17], the corresponding changes in the splenic proteome remain unclear. In this study, we used label-free quantitative proteomics technology to analyze the splenic proteome of GX0101-infected chickens. Based on the involved pathways of inflammation, apoptosis, and tumor in MDV infection, we screened for related signaling pathways and differential proteins (DEPs) in the chicken spleen after 30 and 45 days post-infection (dpi).

## Materials and methods

### Animal experiments and sample preparation

MDV GX0101 was donated by the College of Veterinary Medicine, Shandong Agricultural University, China. The animal experiments were conducted following the protocols of the Ethical and Animal Welfare Committee of the Key Laboratory of Animal Immunology, Ministry of Agriculture, China [18]. SPF chicken embryos were purchased from Zhengzhou Ruixiang Hatchery, China. A total of 32 one-day-old SPF chickens were divided into the control ( $n=4$ ) and experimental ( $n=28$ ) groups. Additionally, the experimental group had 7 sub-groups ( $n=4$ ). Each chick in the experimental group was intraperitoneally injected with chicken embryo fibroblasts (CEFs) containing 2000 PFU GX0101, while control chickens were injected with equal doses of CEF cultures. The chickens in the experimental and control groups were fed in two SPF isolators with the same environmental conditions, and their deaths and mental states were recorded. According to the 2020 edition of the American Veterinary Medical Association Guidelines for the Euthanasia of Animals, chickens were anesthetized intravenously with sodium pentobarbital (30 mg/kg) and then exsanguinated to death at 7, 14, 21, 30, 45, 60, and 90 dpi, respectively. All blood and tissue samples from the heart, liver, spleen, lung, kidney, and glandular stomach tissues were collected in sterile tubes, snap-frozen in liquid nitrogen, and then stored at  $-80^{\circ}\text{C}$  for further use. These samples were examined for histopathology, real-time PCR, and label-free quantitative proteomics. The histological samples were fixed in 4% neutral paraformaldehyde for more than 15 days.

### DNA extraction and viral load estimation by qPCR

The animal blood samples were collected at 7, 14, 21, 30, 45, 60, and 90 dpi in the experimental groups. The viral genome was extracted from blood using the Whole Blood Genomic DNA Extraction Kit (TransGen, China). The *meq* and *gB* recombinant plasmids were constructed. The absolute quantitative standard curves of *meq* and *gB* were established by qPCR by comparing levels with standard plasmids as described previously [19]. The serum expression levels of *meq* and *gB* were detected by qPCR and, the data were analyzed by the absolute quantitative method. qPCR was performed on a LightCycler 96 (Roche, Switzerland) instrument, using water as a negative control. Each reaction volume was 20  $\mu\text{L}$ , including 10  $\mu\text{L}$  SYBR Premix Ex Taq<sup>TM</sup> (Vazyme, China), 0.5  $\mu\text{L}$  forward primer (10 mM), 0.5  $\mu\text{L}$  reverse primer (10 mM), 1.0  $\mu\text{L}$  DNA template and 8  $\mu\text{L}$  ddH<sub>2</sub>O. The primer sequences used are listed in Table 1. The temperature program was as follows: 95  $^{\circ}\text{C}$  for 120s, 95  $^{\circ}\text{C}$  for 15s, 60  $^{\circ}\text{C}$  for 60s (35 cycles), and 72  $^{\circ}\text{C}$  for 20s. Triplicate datasets

**Table 1** The sequences of primers used in this study

Name	Primer sequence(5'-3')	Size	NCBI No.
<i>meq</i>	Sense: ACGCTCAGCTTTGTCTGT	181	JX844666.1
	Antisense: GGAAACCACAGACCGTAGA		
<i>gβ</i>	Sense: CCGCTCTGTGTTCCGTATT	191	JX844666.1
	Antisense: TGACTGGAAGGCTTCTTTT		
<i>GAPDH</i>	Sense: TGGGTGTAACCATGAGAAA	171	NM_204305.2
	Antisense: CATCCACCGTCTTCTGTGTG		
<i>PRNP</i>	Sense: ACCGATGGTGGAGTGAGAAC	221	GU991271.1
	Antisense: GGATCACCTTCTGACCACT		
<i>IFNLR1</i>	Sense: AGCCGGATCTGAAGACAAGA	156	NM_001389541.2
	Antisense: CACACTGGCTGGGAGAATT		
<i>FN1</i>	Sense: TTTGGGTATGCAGTGGTTGA	159	NM_001198712.2
	Antisense: GTCCTCCGTTGTAGGTGAA		
<i>CTSD</i>	Sense: CCAAGGAAGTGAAGGAGCTG	190	NM_205177.2
	Antisense: CTCAGGCAGATGGTCTCTCC		
<i>CD79B</i>	Sense: ACGGGAACAGCACCAGTAAC	170	NM_001006328.3
	Antisense: CACGTGGAACCTCTTCCAT		
<i>IL2RA</i>	Sense: CGAAGCAAGCAAACAATTCA	169	NM_204596.2
	Antisense: TCCACATTCTGACGTGAT		
<i>MAVS</i>	Sense: GGGACATCCAGCACAGTTTT	174	AB772011.1
	Antisense: AGCACTCAAATCCCTTGGTG		
<i>STAT1</i>	Sense: CAGATGGAAGTGGGAGGTGT	208	NM_001012914.2
	Antisense: CCTCTTGTGATGCACCATTTG		
<i>STAT3</i>	Sense: TTGGAACAGATGCTCACAGC	184	NM_001030931.2
	Antisense: TCAAGCCGGTCTAAGCAGAT		

were analyzed using LightCycler<sup>®</sup> 96 software (version 1.1.0.1320).

### Histopathology

The heart, liver, spleen, lung, kidney, and glandular stomach tissues were fixed in a 4% formaldehyde solution to make paraffin-embedded sections of 5 μm. The tissue sections were stained with hematoxylin and eosin and examined under a light microscope (Leica DM750) as described previously [20].

### Protein extraction, reductive alkylation, trypsin digestion, and LC-MS/MS analysis

Proteins were extracted from respective spleen tissues at 30 dpi and 45 dpi for crude analysis. The four duplicate samples in each group were mixed up. All samples were transferred to a centrifuge tube and centrifuged at 10,000×g for 30 min at 4°C. Lysis buffer was then added to extract total proteins. The proteins were precipitated with trichloroacetic acid and centrifuged at 40,000×g for 30 min at 4°C. The protein concentration was determined using the Qubit fluorescent protein quantification kit (Invitrogen, China). The processing of protein samples and LC-MS/MS analysis were performed as described previously [21].

### Differential expression analysis

Tandem mass spectra were searched against Mascot 2.1 (local host) chickens protein databases. The search results were filtered using a cutoff of 1% peptide false identification rate (Peptide FDR). The peptides with a Z score < 4 or a delta-mass > 5 ppm were rejected. Additionally, the minimum number of peptides needed to identify a protein was set to 1. We used the Quantitative Software Profile Analysis 2.0 program with default parameters for data analysis. DEPs were screened with a threshold of 1.5-fold change (FC = fold change). DEPs with FC ≥ 1.5 were considered upregulated, those with FC ≤ 0.667 were downregulated, and those with 0.667 < FC < 1.5 were deemed to have no significant change in their levels.

### Gene ontology (GO) and Kyoto encyclopedia of genes and genomes (KEGG) enrichment analyses of DEPs

GO analysis of DEPs was performed through the Evolutionary Relationships (PANTHER) database version 6.1 (www.pantherdb.org). The GO enrichment analysis first mapped all DEPs to each term of the GO database (<http://www.geneontology.org/>) and then calculated the number of proteins per term. After that, it applied a hypergeometric test to identify GO entries that were significantly enriched in DEPs compared with the background proteins, and their *P*-values were calculated. GO terms with a corrected *P* value ≤ 0.05 were considered significantly enriched by DEPs.

Signaling pathway analysis was performed with the KEGG database (<http://www.genome.jp/kegg/pathway.html>), similar to the GO enrichment analysis. Pathways with a *P*-value ≤ 0.05 were considered significantly enriched by DEPs.

### Protein-protein interaction networks (PPI) and clustering analysis of DEPs

The PPI networks (confidence score ≥ 0.40) of DEPs were obtained using the STRING database (<https://string-db.org/>) and visualized by Cytoscape software (v3.7.2) to perform the clustering analysis as described previously [22].

### Real-time PCR

Total RNA was extracted from the spleen tissues using the Ultrapure RNA Kit, including DNase I (ComWin, Beijing, China). The cDNA was synthesized using the TransScript First-Strand cDNA Synthesis SuperMix kit (TransGen, Beijing, China) following the manufacturer's protocol. Primers were designed by Prime 5.0 software based on the gene sequences from the NCBI (Table 1). Reaction volume, procedures, instruments, and software were similar to those above mentioned for qPCR. The relative expression values of genes were calculated using

the  $2^{-\Delta\Delta C_t}$  method and normalized to GAPDH, an internal reference gene [23].

### Statistical analysis

Statistical analysis was performed using IBM SPSS, version 25.0 (Chicago, IL). A one-way analysis of variance (ANOVA) was used to detect statistical differences between the control and the experimental groups.

## Results

### Serum viral load at different periods of infection

As shown in Fig. 1A, B, both *gB* and *meq* exhibited similar expression trends, which peaked at 21 dpi after the GX0101 infection. Subsequently, their levels slumped to the bottom at 30 dpi and then rapidly increased to the maximum at 45 dpi. From thereon, the expression level gradually decreased to 90 dpi and remained at a low level.

### Pathological manifestations of organs in infected chickens

The microscopical images showing the histopathology of tissue sections are shown in Fig. 2. Compared with the control group, the normal organizational structure of the internal organs in experimental chickens was compromised by tumor tissue at 45 dpi. Neoplastic cells exhibited pleomorphism with darker cytoplasmic staining, less cytoplasm, heteromorphic nuclei, a low degree of differentiation, and a visible abnormal mitotic phase. The liver demonstrated local congestion, diffuse tumor cell proliferation, hepatocyte cord swelling, hepatic sinusoidal atrophy, and local lymphocyte proliferation. The lungs had local congestion and hemorrhage, widening of the pulmonary interstitium, and significant lymphocyte proliferation, accompanied by tumor cell proliferation.

The spleen structure was severely damaged, the white pulp lymphocytes were significantly reduced, and there were some necrotic cells. The kidney showed interstitial congestion and renal tubular epithelial cells were degenerated and necrotized. Also, the renal interstitium had tumor cell proliferation. The heart showed clear lesions with tumor cell proliferation along with myocardial fibrosis and inflammatory cell infiltration. The myocardial membrane was ruptured with interstitial edema. The glandular stomach exhibited severe lymphocyte proliferation in the lamina propria, accompanied by tumor cell hyperplasia and the destruction of the original structure. Meanwhile, no obvious histopathological changes were observed in the liver, spleen, and kidney at 30 dpi in the experimental group as in the control group.

### Analysis of total DEPs

In this study, we selected DEPs based on  $FC > 1.5$  with a  $P$ -value  $\leq 0.05$ . Compared with the control group, in total, 2904 DEPs were identified in both 30 and 45 dpi samples. Splenic proteomic analysis revealed 1660 (891 upregulated and 769 downregulated) and 1244 (687 upregulated and 557 downregulated) DEPs at 30 and 45 dpi, respectively, compared with the uninfected spleen tissues (Fig. 3A). Among the DEPs, 852 and 436 were unique to 30 and 45 dpi, respectively. Meanwhile, there were 808 shared DEPs between 30 and 45 dpi samples (Fig. 3B).

### GO analysis of DEPs

To fully analyze the potential cellular function associated with DEPs, we performed GO functional enrichment

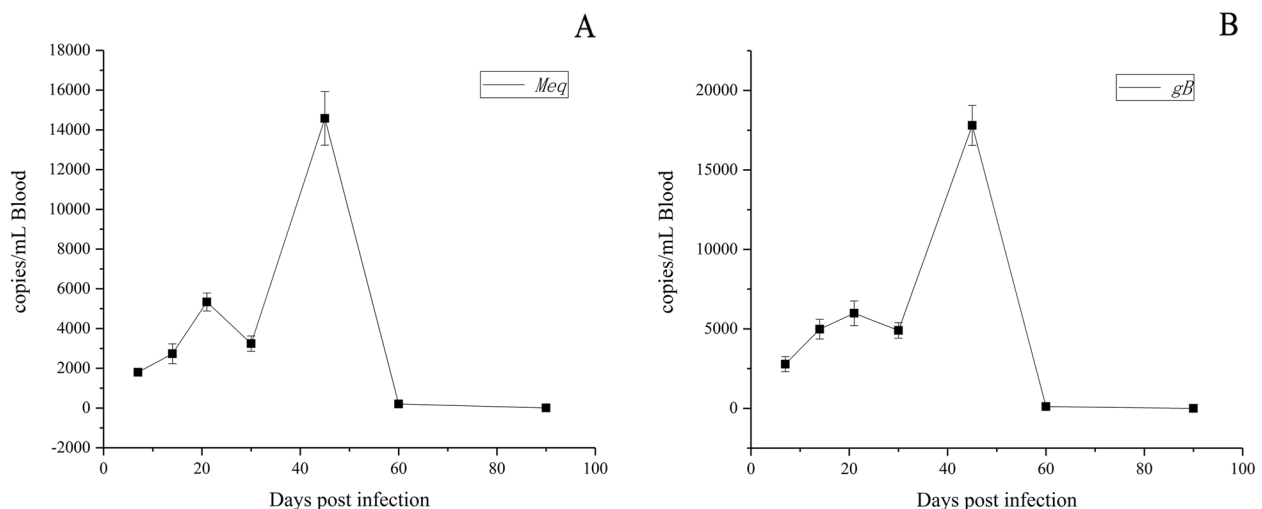


**Fig. 1** The qPCR detection of *meq* and *gB* gene expressions in chicken blood after MDV infection. The change in serum expression of (A) *meq* and (B) *gB* after MDV infections

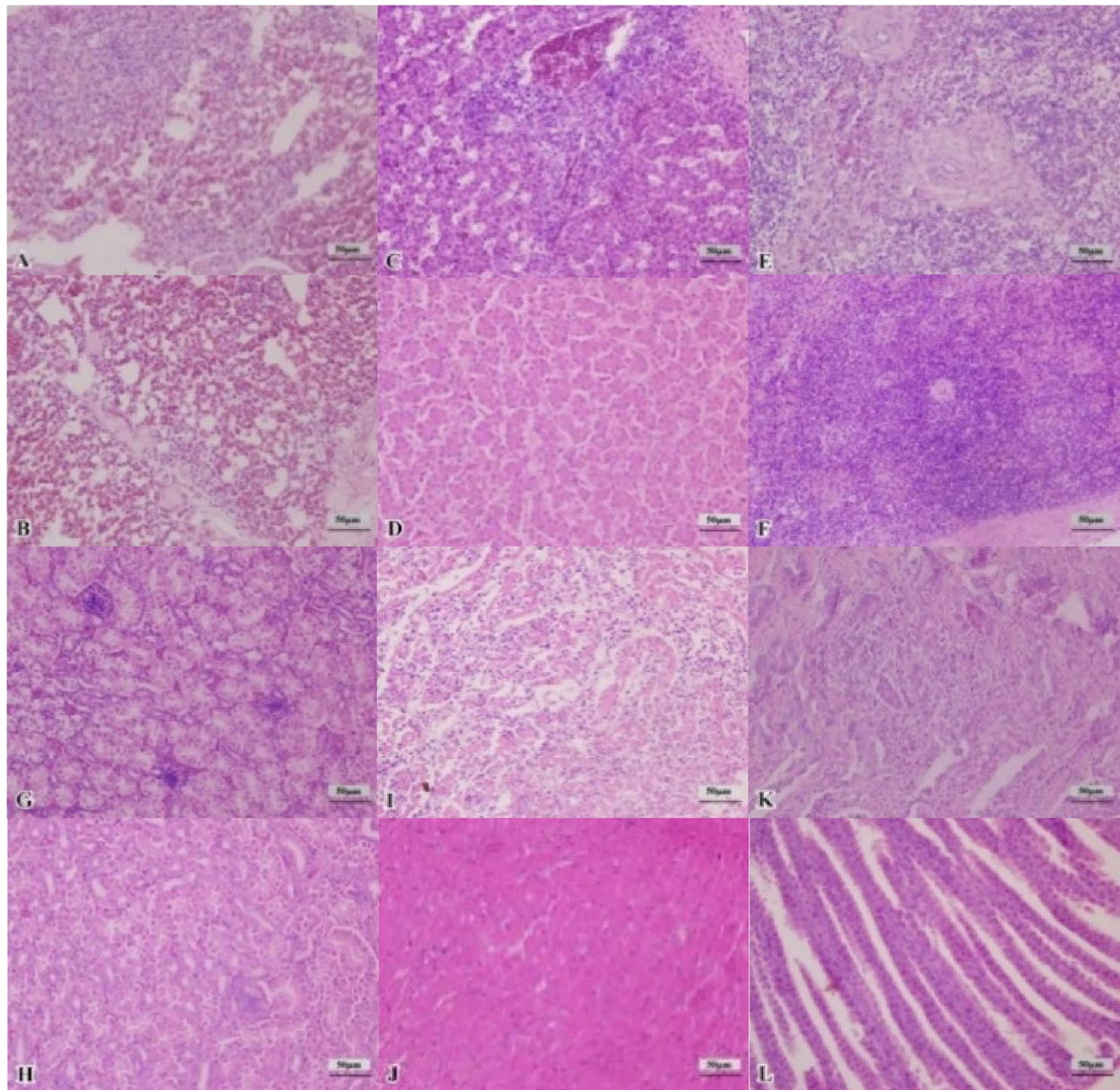


**Fig. 2** Histopathologic observation of chickens (400x) at 45 dpi. **A, C, E, G, I, and K:** Pathological observation of lung, liver, spleen, kidney, heart, and glandular stomach in MDV-infected tumor-diseased chickens. **B, D, F, H, J, and L:** Pathological observation of lung, liver, spleen, kidney, heart, and glandular stomach in the healthy control group

analysis (Fig. 3C, D). The DEPs were mainly involved in intracellular molecular and ion binding, cellular component organization, cellular processes, and biological regulation.

#### KEGG enrichment analysis

To explore the KEGG pathways linked to inflammation, apoptosis, and tumors, we screened 34 relevant signaling pathways related to DEPs identified at 30 dpi and 33

relevant signaling pathways related to DEPs identified at 45 dpi (Fig. 4A, B). These pathways included the Toll-like receptor, mTOR, AMPK, FoxO, B cell receptor, Jak-STAT, cAMP, Apoptosis, T cell receptor, TNF, Chemokine, PPAR, MAPK, Notch, PI3K-Akt, ErbB, Rap1, cGMP-PKG, VEGF, Calcium, Wnt, NF- $\kappa$ B, Ras, Hippo, Prion diseases, and Fc epsilon RI signaling pathway. The TGF-beta pathway was associated only with DEPs identified in 30 dpi samples.

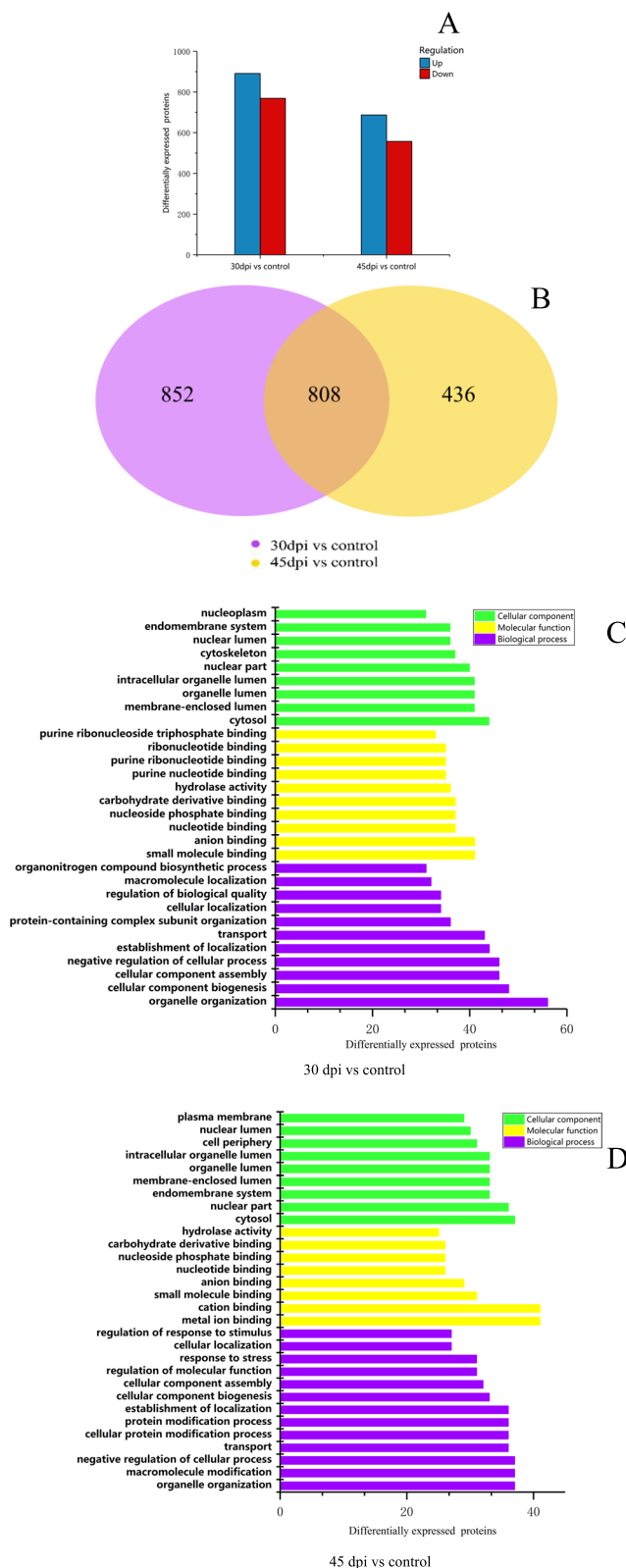


**Fig. 3** Proteomic data analysis. **A** Protein expression differences of MDV-infected chickens at 30 and 45 dpi. Fold Change > 1.5 and a Fold Change < 0.667 was the threshold. The blue plots represent upregulated DEPs (Fold Change > 1.5) and the red plots represent downregulated DEPs (Fold Change < 0.667). **B** Venn diagram of total DEPs. Purple represents the 30 dpi group. Yellow represents the 45 dpi group. GO functional enrichment pathway of **(C)** 30 dpi and **(D)** 45 dpi

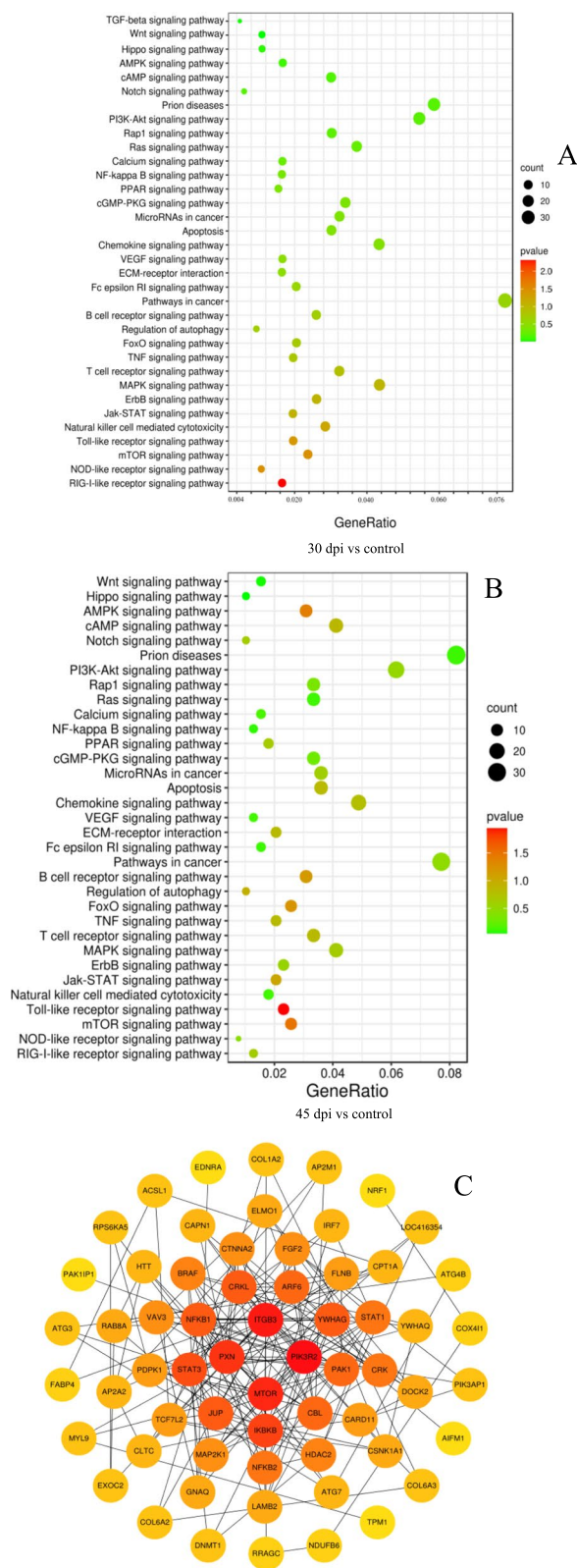


**Fig. 4** Enrichment analysis of selected DEPs in the splenic proteome of GX01010-infected chickens. KEGG enrichment analysis of selected DEPs in (A) 30 dpi and (B) 45 dpi groups. C The protein–protein interaction (PPI) networks of DEPs at the 30 and 45 dpi in the KEGG pathway

**PPI network and clustering analyses of DEPs**

We observed that different DEPs were in the same signal pathway (Table 2). There were 83 shared DEPs in the signal pathways of the 30 dpi and 45 dpi experimental groups. A PPI network of 83 DEPs, with 62 nodes and 191 edges, was constructed using the STRING database and visualized by Cytoscape (v3.7.2) (Fig. 4C). In the PPI network, the top hub proteins were *ITGB3*, *PIK3R2*, *MTOR*, *PXN*, *IκB*, *JUP*, *STAT3*, *NFKB1*, *CRKL*, and *ARF6*.

**qPCR validation of proteomic data**

We used qPCR to validate the proteomic data by estimating the mRNA expressions of selected DEPs. As shown in Fig. 5A, B, the mRNA expressions of *FN1*, *CD79B*, *STAT1*, and *STAT3* were considerably downregulated, whereas those of *IFNLRI*, *CTSD*, and *MAVS* were significantly upregulated. These expression results were consistent with proteomic data. Notably, the qPCR result of *IL2RA*, i.e., upregulation of *IL2RA*, was different from the proteome results. Also, the expression of *PRNP* varied with MDV infection and infection time (Fig. 5C).

**Discussion**

In recent years, the emergence of targeted gene and protein expression profiles has facilitated a better understanding of host responses to MDV. Moreover, modern techniques and tools for analyzing host cell proteomes and transcriptomes have accelerated the exploration of complex interactions between the host and the pathogen. We observed that in chickens infected with GX0101, the serum load of MDV reached its peak at 45 dpi. Histopathology revealed the destruction of the normal organizational structure of the internal organs in the experimental chickens at 45 dpi, characterized by the presence of tumor tissue. Notably, the spleen structure suffered severe damage, with a significant reduction in lymphocytes in the white pulp.

We then conducted proteome analysis of spleen tissue at 30 and 45 dpi, which laid the foundation for subsequent studies on MDV strain GX0101. In this study, we identified 1660 and 1244 DEPs at 30 dpi and 45 dpi, respectively, using the label-free quantitative proteomics technology. Notably, a previous study on splenic protein expression in MDV strain RB1B-infected chickens, employing 2-DE and MS, identified only 58 DEPs

**Table 2** KEGG pathway enrichment analysis of DEPs identified at 30 dpi and 45 dpi of MDV

KEGG pathway	Common proteins		Specific proteins	
	Common proteins	30 dpi specific proteins	30 dpi specific proteins	45 dpi specific proteins
RIG-I-like receptor signaling pathway	IRF7/NFKB1/NLRX1/IkBKB/RELA/NFKB1/IkBKB/RELA	TRIM25/MAVS/ATG5 FNI1/MAPK1		
NOD-like receptor signaling pathway	IkBKB/MTOR/PIK3R2/PDPK1/CAB39/RRAGC/BRAF/PIK3R2/BRAF/MAP2K1/PPP3R1/VAV3/PAK1	PRKCA/RPS6KA1/MAPK1 PTPN11/LOC419429/BF1/MAPK1/PRKCA/STAT5B/STAM2/PTPN11/LOC419429/		PRKAA1/RICTOR
Natural killer cell mediated cytotoxicity	MTOR/PIK3R2/STAT1/STAT3/NFKB1/IkBKB/RELA/BRAF/MAP2K1/PPP3R1/PAK1/CRK/RPS6KA5/NFKB2/FLNB/FGF2	PLA2G4A/LAMTOR3/STMN1/ATF2/MAPK1/PRKCA/RPS6KA1		CNTRF/IFNLR1/IL2RA/ MAP2K6/RRAS2/RAP1B/
Jak-STAT signaling pathway	NFKB1/IkBKB/RELA/PIK3R2/PDPK1/MAP2K1/PPP3R1/VAV3/PAK1/CBL/CARD11	PRKCO/MAPK1		NFKBIE/
MAPK signaling pathway	IkBKB/PIK3R2/PDPK1/BRAF/MAP2K1/STAT3/NFKB1/IkBKB/RELA/PIK3R2/MAP2K1/PPP3R1/VAV3/CARD11/PIK3AP1	CAT5GK3/MAPK1 BTK/MAPK1		PRKAA1/PCK2/SOD2/ NFKBIE/CD79B/
FoxO signaling pathway	NFKB1/IkBKB/RELA/MTOR/PIK3R2/BRAF/STAT1/MAP2K1/STAT3/CBL/CRK/NFKB2/FGF2/CTNNA2/HDAC2/GNAO1/LAMB2/LOC416354/JUP/EDNRA/CCDC6/TCF7L2	RASSF5/FNI1/MAPK1/PRKCA/STAT5B/COL4A2/TPM3/ITGA3/GNG5/ARNT/SLC2A1		GNAI2/ITGA2/FN1/TCEB1/APPL1/
Pathways in cancer	PIK3R2/MAP2K1/PPP3R1/PXN/LAMB2/ITGB3/COL6A2/COL1A2/NFKB1/IkBKB/RELA/PIK3R2/BRAF/STAT1/MAP2K1/VAV3/PAK1/STAT3/CRK/CRKL/PXN/DOCK2/ELMO1	MAPK1/PRKCA/PLA2G4A COL4A2/ITGA3/CD44 MAPK1/STAT5B/GNG5/WASL		ITGA2/FN1/THBS1/ GNAI2/RAP1B/XCL1/
VEGF signaling pathway	NFKB1/IkBKB/RELA/PIK3R2/PDPK1/MAP2K1/TUBA1C/AIFM1/BAK1/CAPN1	MAPK1/LMN1/LMNA/		TUBA3E/CTSD/DFFA/
ECM-receptor interaction	NFKB1/IkBKB/MTOR/MAP2K1/STAT3/CRK/CRKL/RPS6KA5/ITGB3/BAK1/DNMT1/TPM1/	PRKCA/STMN1/CD44		THBS1/EZR/
Chemokine signaling pathway	PIK3R2/MAP2K1/PPP3R1/GNAQ/EDNRA/SLC25A6/ATP1B1/MYL9/GUCY1A2/PRKG1/	MAPK1/ATF2/SLC25A4/PPP1CB/ATP2B1		ATP1A3/GNAI2/
Apoptosis	PDPK1/CPT1A/FABP4/ACSL1/NFKB1/IkBKB/RELA/NFKB2/CARD11/	ACAA1/ILK/CPT2 TRIM25/PRKCO/BTK		PCK2/FABP7/FABP5/
MicroRNAs in cancer	PPP3R1/GNAQ/EDNRA/SLC25A6/STIM1/NFKB1/IkBKB/RELA/PIK3R2/MAP2K1/PAK1/FGF2/EXOC2/ARF6/	PRKCA/SLC25A4/ATP2B1 MAPK1/PRKCA/PTPN11/LOC419429/PLA2G4A/RASSF5/GNG5		P2RX1/ RRAS2/RAP1B/RAB5B/
cGMP-PKG signaling pathway	PIK3R2/BRAF/MAP2K1/CRK/CRKL/FGF2/GNAQ/ITGB3/	MAPK1/PRKCA/RASSF5/TLN2/		MAP2K6/GNAI2/RAP1B/THBS1/
PPAR signaling pathway	NFKB1/IkBKB/RELA/MTOR/PIK3R2/PDPK1/MAP2K1/FGF2/PIK3AP1/LAMB2/ITGB3/COL6A2/COL6A3/COL1A2/YWHAQ/YWHAG/HDAC2/LOC416354/SNW1/	FNI1/MAPK1/PRKCA/ATF2/SGK3/COL4A2/ITGA3/GNG5		PRKAA1/PPP2R5C/PCK2/IL2RA/ITGA2/FN1/THBS1/
NF-kappa B signaling pathway				PSEN1/
Calcium signaling pathway				
Ras signaling pathway				
Rap1 signaling pathway				
Notch signaling pathway				



**Table 2** (continued)

KEGG pathway	Common proteins	Specific proteins	
		30 dpi specific proteins	45 dpi specific proteins
cAMP signaling pathway	NFKB1/RELA/PIK3R2/ BRAF/MAP2K1/NAV3/ PAK1/ EDNRA/ATP1B1/ MYL9/	MAPK1/ PPP1CB/ ATP2B1	RRAS2/ATP1A3/ GNAI2/RAP1B/ CNGA3/
AMPK signaling pathway	MTOR/PIK3R2/PDPK1/ CAB39/CPT1A/RAB8A/PFKM/		PRKAA1/PPP2R5C/RAB11B/PCK2/
Hippo signaling pathway	CTNNA2/TCF7L2/ YWHAQ/YWHAG/	PPP1CB	
Wnt signaling pathway	PPP3R1/LOC416354/TCF7L2/CSNK1A1/	PRKCA	PSEN1/TBL1X/
Prion diseases	MAP2K1/PPP3R1/ HDAC2/GNAQ/CAPN1/ SLC25A6/C7/C6/ CLTC/AP2M1/ATP8/ COX4I1/ NDUFB6/DCTN2/AP2A2/HTT/ DCTN4/NRF1/ POLR2F/ UBE2G1/UCHL1	MAPK1/ SLC25A4/ COX7A2/ NDUFV1/ NDUFB3/ SEP-05	SOD2/GNAI2/ PSEN1/NDUFA9/ NDUFB10/LRPT1/ UBE2G2/CLTA/ TGM2/ POLR2L
Fc epsilon R1 signaling pathway	PIK3R2/PDPK1/ MAP2K1/NAV3/	MAPK1/PRKCA/BTK/PLA2G4A	MAP2K6/
Regulation of autophagy	ATG7/ATG3/ATG4B/ ATG4B/	ATG5	PRKAA1/
TNF signaling pathway	NFKB1/ IκBKB/RELA/ PIK3R2/MAP2K1/ RPS6KA5/	MAPK1/ATF2/	MAP2K6/
Toll-like receptor signaling pathway	IRF7/NFKB1/ IκBKB/ RELA/PIK3R2/STAT1/ MAP2K1/	MAPK1	MAP2K6/
ErbB signaling pathway	MTOR/PIK3R2/ BRAF/ MAP2K1/PAK1/ CBL/CRK/ CRKL/	MAPK1/PRKCA/ STAT5B	
TGF-beta signaling pathway		MAPK1/ E2F4	

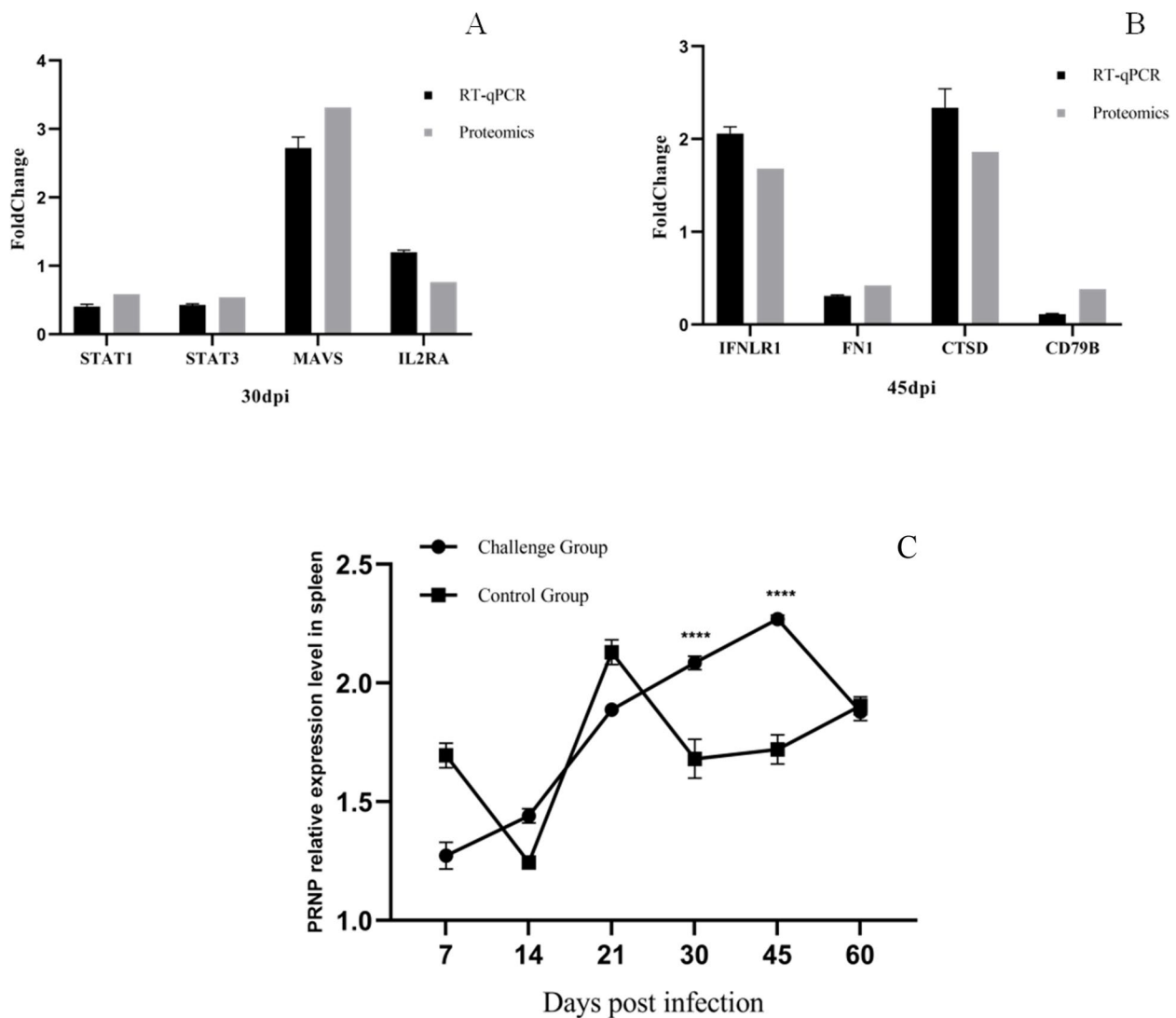


**Fig. 5** The RT-qPCR validation of DEPs. RT-qPCR validation of DEPs at (A) 30 dpi and (B) 45 dpi. (C) RT-qPCR detection of *PRNP* expression at 7, 14, 21, 30, 45, and 60 dpi. *GAPDH* was the internal reference gene. \*\*\* $P < 0.01$

[9]. Additionally, a study combining 2-DE and MS analysis of the splenic proteomics of genetically resistant and susceptible chickens infected with MDV strain JM-16 identified only 40 DEPs [11]. While several MDV strains have been analyzed for splenic proteomics, these prior studies primarily utilized 2-DE and MS. In contrast, the label-free quantitative proteomics technology employed in our study offers higher resolution and accuracy.

To investigate the mechanism of splenic tissue damage caused by MDV in chickens, we analyzed KEGG pathways related to inflammation, apoptosis, and tumor based on the proteomic results. The results revealed that the signaling pathways were consistent in both the 30

dpi and 45 dpi experimental groups, but there were differences in DEPs. The pathways linked to inflammation and apoptosis in both groups included Toll-like receptor, FoxO, B cell receptor, AMPK, regulation of autophagy, apoptosis, T cell receptor, TNF, PPAR, Notch, RIG-I-like receptor, PI3K-Akt, NOD-like receptor, Calcium, cGMP-PKG, natural killer cell-mediated cytotoxicity, NF- $\kappa$ B, and Fc epsilon RI pathway.

In primary lymphoid organs such as the bursa, thymus, and spleen, MDV initially replicated in B cells and then infected T cells through direct intercellular transfer, ultimately causing T-cell lymphoma [24]. This finding is consistent with our results, indicating that both the T-cell and B-cell receptor pathways play a role in altering protein

expression in tumor formation. Furthermore, the pathways linked to GX0101-induced tumors in both the 30 dpi and 45 dpi experimental groups included mTOR, MAPK, cAMP, ECM-receptor interaction, Chemokine, JAK-STAT, MicroRNAs in cancer, ErbB, pathways in cancer, Rap1, VEGF, Ras, Wnt, Prion diseases, and Hippo pathway. The MAPK pathway, a tumorigenesis-related pathway that is critical for inflammation and cancer development, was also identified [25, 26]. Notably, the MAPK pathway has also been implicated in previous MD studies [27, 28].

The transcriptome analysis of the chicken infected with the RB1B strain of MDV uncovered alterations in tumor-related pathways, such as the WNT signaling pathway, JAK-Stat signaling pathway, Notch signaling pathway, MAPK signaling pathway, and TGF-Beta signaling pathway [29]. The TGF-beta signaling pathway was linked to MDV tumorigenesis [30]. Nonetheless, in our study, the TGF-beta pathway displayed DEPs at 30 dpi, but no DEP was found at 45 dpi, suggesting that the TGF-beta pathway might only be implicated in the early and middle stages of viral infection. We conducted PPI network analysis for DEPs in the selected pathway at 30 and 45 dpi. We screened several hub proteins, including ITGB3, PIK3R2, MTOR, PXN, I $\kappa$ B, JUP, STAT3, NFKB1, CRKL, and ARF6. The ITGB3 protein, known as the integrin beta chain beta 3, was identified as an epithelial-to-mesenchymal transition biomarker in colorectal cancer, prostate cancer, and breast cancer [31, 32]. ITGB3 influences tumor immunity through both the innate and adaptive immune systems. TGB3 could function as a regulator to enhance TGF- $\beta$ /H<sub>2</sub>O<sub>2</sub>/HOCl signaling, thereby transforming non-metastatic tumors into metastatic tumors [33]. Activated macrophages exerted anti-tumor effects by producing inflammatory cytokines like IL-1 $\beta$ , while the interaction between ITGB3 and MFGE8 inhibited macrophage IL-1 $\beta$  production by inducing necrotic cells and an ATP-dependent manner [34]. The PIK3R2 protein serves as a regulatory component of PI3K, and targeting PIK3R2 could inhibit the proliferation, migration, and invasion of NSCLC A549 cells by modulating the PTEN/PI3K/AKT pathway [35]. MTOR exists in two complexes, MTORC1 and MTORC2. MTORC1 controls protein synthesis, cell growth, and proliferation, while MTORC2 regulates the actin cytoskeleton, promoting cell survival and cell cycle progression [36, 37]. MTOR plays a crucial role in tumor progression, and mTOR inhibitors have been employed in clinical cancer treatment [38]. PXN, a cytoskeletal protein, when overexpressed, facilitated tumor progression and acted as an oncogene by regulating Bcl-2 [39]. In hepatocellular carcinoma, ITGB1 regulated the cell cycle process via the PXN/YWHAZ/AKT pathway, promoting hepatocellular carcinoma progression [40]. Overexpressing JUP, a homolog of  $\beta$ -catenin, reduced the expression

of oncogenic STAB1 [41]. V-Crk avian sarcoma virus CT10 oncogene homolog-like (CRKL) acts as an adaptor protein of the Crk family and participates in cell proliferation, adhesion, and migration [42]. Moreover, CRKL regulates the activity of Ras, JNK, and Stat5 signaling pathways [43, 44]. CRK is overexpressed in various cancers, and its expression often correlates with tumor grade [45]. Arf6 belongs to the small GTPases ADP-ribosylation factor (Arf) family. Studies have established a significant correlation between the activation and high expression of Arf6 protein and the invasion and metastasis of several tumors. Inhibiting Arf6 activity could inhibit tumor invasion and metastasis [46, 47]. STAT3 serves as the convergence point of multiple cancer-related pathways and is frequently overactivated in cancer progression [48]. NF- $\kappa$ B1 is a major component of NF- $\kappa$ B. Many cancers are marked by the elevated activity of NF- $\kappa$ B, which serves as a survival factor for malignant cells due to its major anti-apoptotic function [49]. NF- $\kappa$ B and STAT3 cooperatively promote tumor development through functional interactions, inducing pro-tumor genes, including genes that generate anti-apoptotic chemokines and immunosuppressive cytokines [50–52]. I $\kappa$ B encodes I $\kappa$ B kinase  $\beta$ , which facilitates I $\kappa$ B degradation and mediates key steps in NF- $\kappa$ B activation [53, 54]. These hub proteins were intricately connected to tumor development and warrant further investigation in MD.

PrP<sup>C</sup> (cellular prion protein) is encoded by PRNP. When it misfolds into PrP<sup>Sc</sup> (scrapie isoform of prion protein) and accumulates in neuronal cells, it leads to prion disease [55]. Compared to adjacent non-tumor tissues, PrP<sup>C</sup> expression was found to be upregulated in various cancer tissues, including colorectal cancer [56], gastric cancer [57], and pancreatic cancer [58]. Our laboratory confirmed the correlation between MDV infection and PRNP expression at the cellular level and in the tissues of naturally developed MD chickens [59, 60]. This result aligns with the present study. A transcriptomic study highlighted three differentially expressed genes, *TCRB*, *HSP70*, and *XCL1*, between MDV-infected resistant and susceptible chickens. Therefore, they represent key targets for future studies elucidating the mechanisms of MD resistance [61]. Our proteome results revealed that *TCRB* and *HSP70* protein expression remained unchanged, while *XCL1* expression was upregulated, consistent with a previous study [18]. Furthermore, several members of the HSP40 family (A3, A4, B6, C11, C13) also exhibited changes in this study.

Further analysis uncovered 40 unique DEPs at 45 dpi, mainly involved in cell adhesion (FN1), cell attachment (ITGA2, THBS1), signal transduction (LRP1, TGM2, RRAS2, GNAI2, RAB11B, RAB5B, CLTA), cytoskeleton (EZR), immunity (XCL1, CD79B), transcriptional

regulation (TBL1X, PRKAA1, POLR2L, TCEB1), and apoptosis (DFFA, IL2RA). Among these proteins, THBS1 plays a vital role in tumorigenesis. KEGG analysis showed that THBS1 participates in PI3K-Akt, ECM-receptor interaction, microRNAs in cancer, and the Rap1 pathway. THBS1, a tumor-specific extracellular matrix protein and tumor suppressor, is known to inhibit angiogenesis, regulate anti-tumor immunity, and stimulate tumor cell migration in the tumor microenvironment [62]. In hepatocellular carcinoma cells, upregulation of THBS1 promoted cell proliferation and inhibited apoptosis [63]. In bladder urothelial carcinoma (BLCA), THBS1 counteracted the tumor-associated behavior of miR-19a-3p in BLCA cells [64]. This underscores THBS1 as an important target for tumor therapy, deserving further exploration. It is well-known that tumor cells primarily rely on glycolysis for their energy needs, whereas normal cells predominantly rely on aerobic oxidation. Consequently, glycolytic genes are often overexpressed in tumor cells. Additionally, the qPCR and proteomics results in this study demonstrated that the changes in FN1 and CTSD were consistent with previous transcriptome studies [17].

Many studies have found that PrP is overexpressed in various tumor tissues. This overexpression induces cell proliferation without limits, malignant differentiation, and variations. It affects tumor cell adhesion, invasion, diffusion, apoptosis, and other processes. Additionally, it influences multiple signaling pathways associated with tumor formation. Previous studies conducted in our laboratory revealed that the distribution of the *PRNP* gene in chicken embryos is identical to that in mammals. This suggests that PrP plays a crucial role in the development of chicken embryos and likely serves the same physiological functions in both chicken embryos and mammals [65]. Studies have indicated an upregulation of chicken PrP in the MD tumor cell line, MSB-1) [66]. In bovine mammary epithelial cells, the PrP protein expression increases within 12 hours of *Staphylococcus aureus* infection [67]. Earlier, the fluorescence-quantitative PCR method was used to prove the effect of PRNP expression on MDV infection at the cell level, indicating the relationship between the two. However, the specific mechanism remains unclear. In our study, we confirmed that the expression level of *PRNP* peaked at 30 and 45 dpi in the spleen, closely mirroring the expression trends of *meq* and *gB*.

## Conclusion

The study demonstrates that GX0101 causes significant damage to the spleen. Histopathological examination revealed severe damage to the spleen structure, marked

reduction in white pulp lymphocytes, and necrosis of some lymphocytes in conjunction with tumor cell proliferation. The expression of MDV-related genes peaked at 45 dpi, along with the expression of PRNP. This positive correlation with MDV replication underscores the pivotal role of PRNP in MDV infection. However, the role of THBS1 in MD remains a subject for further investigation. Splenic proteome analysis identified DEPs associated with metabolic pathways related to inflammation, apoptosis, and tumors. This proteomics study lays the groundwork for subsequent research into the interaction between host proteins and MDV strain GX0101.

## Supplementary Information

The online version contains supplementary material available at <https://doi.org/10.1186/s12917-023-03852-5>.

Additional file 1.

## Acknowledgments

The authors would like to thank all the reviewers who participated in the review, as well as MJEditor ([www.mjeditor.com](http://www.mjeditor.com)) for providing English editing services during the preparation of this manuscript.

## Authors' contributions

Zhao Zhang and Chuan Wang were involved in the conception and design of this study. Chuan Wang, Yuanzi Liu, Yuzhe Yang, Man Teng, Xuerui Wan, Zixiang Wu performed the pilot project. Chuan Wang wrote the first draft of the manuscript. All authors were involved in revising, reading, and approving the submitted version of the manuscript.

## Funding

This study was supported by the Subject Construction Funding of Gansu Agricultural University, Gansu Province, China (Grant numbers GSAU-XKJS-2018-074).

## Availability of data and materials

The datasets related to the current study are available at <https://www.iprox.cn/page/home.html>; iProX ID: IPX0006232002.

## Declarations

### Ethics approval and consent to participate

Institutional Review Board Statement: The animal study protocol was approved by the Laboratory Animal Management Committee of Key Laboratory of Animal Immunology, Ministry of Agriculture and Rural Affairs, People's Republic of China, following the protocols of the Laboratory Animal Guidelines for Ethical Review of Animal Welfare permitted by the State Administration for Market Regulation and Standardization Administration of China (permit no. GB/T 35892–2018).

### Consent for publication

Not applicable.

### Competing interests

The authors declare no competing interests.

Received: 16 March 2023 Accepted: 13 December 2023  
Published online: 05 January 2024

## References

- Berthault C, Larcher T, Härtle S, Vautherot JF, Trapp-Fragnet L, Denesvre C. Atrophy of primary lymphoid organs induced by Marek's disease virus during early infection is associated with increased apoptosis, inhibition of cell proliferation and a severe B-lymphopenia. *Vet Res.* 2018;49(1):31. <https://doi.org/10.1186/s13567-018-0526-x>.
- Baigent SJ, Smith LP, Nair VK, Currie RJ. Vaccinal control of Marek's disease: current challenges, and future strategies to maximize protection. *Vet Immunol Immunopathol.* 2006;112(1–2):78–86. <https://doi.org/10.1016/j.vetimm.2006.03.014>.
- Voronin ES, Trubitsyn BI, Dushkin VA. Marek's disease. *Vopr Virusol.* 1972;17(6):656–61.
- Simu G, Ciobanu H, Ciobanu-Bilc A. Histological aspects of lymphoid organs in chickens with Marek's disease. *Morphol Embryol (Bucur).* 1980;26(4):345–7.
- Nazerian K. Oncogenesis of Marek's disease. *Cancer Res.* 1973;33(6):1427–30.
- Davison F, Nair V. Use of Marek's disease vaccines: could they be driving the virus to increasing virulence? *Expert Rev Vaccines.* 2005;4(1):77–88. <https://doi.org/10.1586/14760584.4.1.77>.
- Ross LJ, Sanderson M, Scott SD, Binns MM, Doel T, Milne B. Nucleotide sequence and characterization of the Marek's disease virus homologue of glycoprotein B of herpes simplex virus. *J Gen Virol.* 1989;70(Pt 7):1789–804. <https://doi.org/10.1099/0022-1317-70-7-1789>.
- Turner A, Bruun B, Minson T, Browne H. Glycoproteins gB, gD, and gH/gL of herpes simplex virus type 1 are necessary and sufficient to mediate membrane fusion in a cos cell transfection system. *J Virol.* 1998;72(1):873–5. <https://doi.org/10.1128/JVI.72.1.873-875.1998>.
- Thantrige-Don N, Abdul-Careem MF, Shack LA, Burgess SC, Sharif S. Analyses of the spleen proteome of chickens infected with Marek's disease virus. *Virology.* 2009;390(2):356–67. <https://doi.org/10.1016/j.virol.2009.05.020>.
- Lu Z, Qin A, Qian K, Chen X, Jin W, Zhu Y, et al. Proteomic analysis of the host response in the bursa of Fabricius of chickens infected with Marek's disease virus. *Virus Res.* 2010;153(2):250–7. <https://doi.org/10.1016/j.virusres.2010.08.010>.
- Thantrige-Don N, Parvizi P, Sarson AJ, Shack LA, Burgess SC, Sharif S. Proteomic analysis of host responses to Marek's disease virus infection in spleens of genetically resistant and susceptible chickens. *Dev Comp Immunol.* 2010;34(7):699–704. <https://doi.org/10.1016/j.dci.2010.01.016>.
- Zhang Z, Cui Z. Isolation of recombinant field strains of Marek's disease virus integrated with reticuloendotheliosis virus genome fragments. *Sci China C Life Sci.* 2005;48(1):81–8. <https://doi.org/10.1360/03yc0270>.
- Xu X, Sun A, Cui Y, Cui Z. Comparison of pathogenicity and horizontal transmission ability between recombinant Marek's disease virus field strain with REV-LTR and a very virulent reference strain. *Wei Sheng Wu Xue Bao.* 2009;49(4):540–3.
- Su S, Cui N, Li Y, Yu MX, Zhang T, Cheng Z, et al. Increased horizontal transmission of recombinant Marek's disease virus due to Reticuloendotheliosis virus long terminal repeat is the major competitive advantage of the virus being a prevalent strain. *Front Microbiol.* 2019;10:2842. <https://doi.org/10.3389/fmicb.2019.02842>.
- Su S, Cui N, Cui Z, Zhao P, Li Y, Ding J, et al. Complete genome sequence of a recombinant Marek's disease virus field strain with one reticuloendotheliosis virus long terminal repeat insert. *J Virol.* 2012;86(24):13818–9. <https://doi.org/10.1128/JVI.02583-12>.
- Li Y, Sun A, Su S, Zhao P, Cui Z, Zhu H. Deletion of the Meq gene significantly decreases immunosuppression in chickens caused by pathogenic Marek's disease virus. *Viol J.* 2011;8:2. <https://doi.org/10.1186/1743-422X-8-2>.
- Dang L, Teng M, Li HW, Li HZ, Ma SM, Zhao P, et al. Dynamic changes in the splenic transcriptome of chickens during the early infection and Progress of Marek's disease. *Sci Rep.* 2017;7(1):11648. <https://doi.org/10.1038/s41598-017-11304-y>.
- Teng M, Yu ZH, Zhao P, Zhuang GQ, Wu ZX, Dang L, et al. Putative roles as oncogene or tumour suppressor of the mid-clustered microRNAs in Gallid alphaherpesvirus 2 (GaHV2) induced Marek's disease lymphomagenesis. *J Gen Virol.* 2017;98(5):1097–112. <https://doi.org/10.1099/jgv.0.000786>.
- Wang C, Wu R, Li FD, Liu L, Zhang XL, Zhao CL, et al. Expression patterns of prion protein gene in differential genotypes sheep: quantification using molecular beacon real-time RT-PCR. *Virus Genes.* 2011;42(3):457–62. <https://doi.org/10.1007/s11262-011-0579-7>.
- Feldman AT, Wolfe D. Tissue processing and hematoxylin and eosin staining. *Methods Mol Biol.* 2014;1180:31–43. [https://doi.org/10.1007/978-1-4939-1050-2\\_3](https://doi.org/10.1007/978-1-4939-1050-2_3).
- Yang Z, Zhou J, Zhu L, Chen A, Cheng Y. Label-free quantification proteomics analysis reveals acute hyper-osmotic responsive proteins in the gills of Chinese mitten crab (*Eriocheir sinensis*). *Comp Biochem Physiol Part D Genomics Proteomics.* 2022;43:101009. <https://doi.org/10.1016/j.cbd.2022.101009>.
- Shen S, Kong J, Qiu Y, Yang X, Wang W, Yan L. Identification of core genes and outcomes in hepatocellular carcinoma by bioinformatics analysis. *J Cell Biochem.* 2019;120(6):10069–81. <https://doi.org/10.1002/jcb.28290>.
- Wang C, Zhao CL, Liu L, Wu R, Zhang XL. Expression patterns of Doppel in differential ovine PRNP genotypes: quantification using real-time RT-PCR. *Genet Mol Res.* 2015;14(4):12152–8. <https://doi.org/10.4238/2015.October.9.3>.
- Calnek BW. Marek's disease—a model for herpesvirus oncology. *Crit Rev Microbiol.* 1986;12(4):293–320. <https://doi.org/10.3109/10408418509104432>.
- Dhillon AS, Hagan S, Rath O, Kolch W. MAP kinase signalling pathways in cancer. *Oncogene.* 2007;26(22):3279–90. <https://doi.org/10.1038/sj.onc.1210421>.
- Orton RJ, Sturm OE, Vyshemirsky V, Calder M, Gilbert DR, Kolch W. Computational modelling of the receptor-tyrosine-kinase-activated MAPK pathway. *Biochem J.* 2005;392(Pt 2):249–61. <https://doi.org/10.1042/BJ20050908>.
- Subramaniam S, Johnston J, Preeyanon L, Brown CT, Kung HJ, Cheng HH. Integrated analyses of genome-wide DNA occupancy and expression profiling identify key genes and pathways involved in cellular transformation by a Marek's disease virus oncoprotein, meq. *J Virol.* 2013;87(16):9016–29. <https://doi.org/10.1128/JVI.01163-13>.
- Subramaniam S, Preeyanon L, Cheng HH. Transcriptional profiling of meq-dependent genes in Marek's disease resistant and susceptible inbred chicken lines. *PLoS One.* 2013;8(10):e78171. <https://doi.org/10.1371/journal.pone.0078171>.
- Xuming H. Proteome, transcriptomics and natural immunity mechanism of chicken infected with RB1B strain of Marek's disease virus [D]. Yangzhou University; 2014.
- Xu S, Xue C, Li J, Bi Y, Cao Y. Marek's disease virus type 1 microRNA miR-M3 suppresses cisplatin-induced apoptosis by targeting Smad2 of the transforming growth factor beta signal pathway. *J Virol.* 2011;85(1):276–85. <https://doi.org/10.1128/JVI.01392-10>.
- Deep G, Jain AK, Ramteke A, Ting H, Vijendra KC, Gangar SC, et al. SNAI1 is critical for the aggressiveness of prostate cancer cells with low E-cadherin. *Mol Cancer.* 2014;13:37. <https://doi.org/10.1186/1476-4598-13-37>.
- Lei Y, Huang K, Gao C, Lau QC, Pan H, Xie K, et al. Proteomics identification of ITGB3 as a key regulator in reactive oxygen species-induced migration and invasion of colorectal cancer cells. *Mol Cell Proteomics.* 2011;10(10):M110.005397. <https://doi.org/10.1074/mcp.M110.005397>.
- Feng XX, Liu M, Yan W, Zhou ZZ, Xia YJ, Tu W, et al.  $\beta 3$  integrin promotes TGF- $\beta 1$ /H2O2/HOCl-mediated induction of metastatic phenotype of hepatocellular carcinoma cells by enhancing TGF- $\beta 1$  signaling. *PLoS One.* 2013;8(11):e79857. <https://doi.org/10.1371/journal.pone.0079857>.
- Deroide N, Li X, Lerouet D, Van Vré E, Baker L, Harrison J, et al. MFG8 inhibits inflammasome-induced IL-1 $\beta$  production and limits postischemic cerebral injury. *J Clin Invest.* 2013;123(3):1176–81. <https://doi.org/10.1172/JCI65167>.
- Peng LP. Regarding: MicroRNA-126 targeting PIK3R2 inhibits NSCLC A549 cell proliferation, migration, and invasion by regulation of PTEN/PI3K/AKT pathway. *Clin Lung Cancer.* 2021;22(3):e446–50. <https://doi.org/10.1016/j.clcc.2020.06.009>.
- Saxton RA, Sabatini DM. mTOR signaling in growth, metabolism, and disease. *Cell.* 2017;168(6):960–76. <https://doi.org/10.1016/j.cell.2017.02.004>.
- Jacinto E, Loewith R, Schmidt A, Lin S, Rüegg MA, Hall A, et al. Mammalian TOR complex 2 controls the actin cytoskeleton and is rapamycin insensitive. *Nat Cell Biol.* 2004;6(11):1122–8. <https://doi.org/10.1038/ncb1183>.
- Hua H, Kong Q, Zhang H, Wang J, Luo T, Jiang Y. Targeting mTOR for cancer therapy. *J Hematol Oncol.* 2019;12(1):71. <https://doi.org/10.1186/s13045-019-0754-1>.
- Liu Q, Wang J, Tang M, Chen L, Qi X, Li J, et al. The overexpression of PXN promotes tumor progression and leads to radioresistance in cervical

- cancer. *Future Oncol.* 2018;14(3):241–53. <https://doi.org/10.2217/fon-2017-0474>.
40. Xie J, Guo T, Zhong Z, Wang N, Liang Y, Zeng W, et al. ITGB1 drives hepatocellular carcinoma progression by modulating cell cycle process through PXN/YWHAZ/AKT pathways. *Front Cell Dev Biol.* 2021;9:711149. <https://doi.org/10.3389/fcell.2021.711149>.
  41. Aktary Z, Pasdar M. Plakoglobin represses SATB1 expression and decreases in vitro proliferation, migration and invasion. *PLoS One.* 2013;8(11):e78388. <https://doi.org/10.1371/journal.pone.0078388>.
  42. Birge RB, Kalodimos C, Inagaki F, Tanaka S. Crk and Crkl adaptor proteins: networks for physiological and pathological signaling. *Cell Commun Signal.* 2009;7:13. <https://doi.org/10.1186/1478-811X-7-13>.
  43. Feller SM, Knudsen B, Wong TW, Hanafusa H. Detection of SH3-binding proteins in total cell lysates with glutathione S-transferase-SH3 fusion proteins: SH3 blot assay. *Methods Enzymol.* 1995;255:369–78. [https://doi.org/10.1016/s0076-6879\(95\)55039-9](https://doi.org/10.1016/s0076-6879(95)55039-9).
  44. Matsuda M, Mayer BJ, Hanafusa H. Identification of domains of the v-crk oncogene product sufficient for association with phosphotyrosine-containing proteins. *Mol Cell Biol.* 1991;11(3):1607–13. <https://doi.org/10.1128/mcb.11.3.1607-1613.1991>.
  45. Nishihara H, Tanaka S, Tsuda M, Oikawa S, Maeda M, Shimizu M, et al. Molecular and immunohistochemical analysis of signaling adaptor protein Crk in human cancers. *Cancer Lett.* 2002;180(1):55–61. [https://doi.org/10.1016/s0304-3885\(01\)00763-7](https://doi.org/10.1016/s0304-3885(01)00763-7).
  46. Li R, Peng C, Zhang X, Wu Y, Pan S, Xiao Y. Roles of Arf6 in cancer cell invasion, metastasis and proliferation. *Life Sci.* 2017;182:80–4. <https://doi.org/10.1016/j.lfs.2017.06.008>.
  47. Grossmann AH, Zhao H, Jenkins N, Zhu W, Richards JR, Yoo JH, et al. The small GTPase ARF6 regulates protein trafficking to control cellular function during development and in disease. *Small GTPases.* 2019;10(1):1–12. <https://doi.org/10.1080/21541248.2016.1259710>.
  48. Zou S, Tong Q, Liu B, Huang W, Tian Y, Fu X. Targeting STAT3 in Cancer immunotherapy. *Mol Cancer.* 2020;19(1):145. <https://doi.org/10.1186/s12943-020-01258-7>.
  49. Karin M. NF-kappaB and cancer: mechanisms and targets. *Mol Carcinog.* 2006;45(6):355–61. <https://doi.org/10.1002/mc.20217>.
  50. Bollrath J, Gretchen FR. IKK/NF-kappaB and STAT3 pathways: central signaling hubs in inflammation-mediated tumour promotion and metastasis. *EMBO Rep.* 2009;10(12):1314–9. <https://doi.org/10.1038/embor.2009.243>.
  51. Atkinson GP, Nozell SE, Benveniste ET. NF-kappaB and STAT3 signaling in glioma: targets for future therapies. *Expert Rev Neurother.* 2010;10(4):575–86. <https://doi.org/10.1586/ern.10.21>.
  52. Fan Y, Mao R, Yang J. NF-kB and STAT3 signaling pathways collaboratively link inflammation to cancer. *Protein Cell.* 2013;4(3):176–85. <https://doi.org/10.1007/s13238-013-2084-3>.
  53. DiDonato JA, Hayakawa M, Rothwarf DM, Zandi E, Karin M. A cytokine-responsive I-kappaB kinase that activates the transcription factor NF-kappaB. *Nature.* 1997;388(6642):548–54. <https://doi.org/10.1038/41493>.
  54. Mercurio F, Zhu H, Murray BW, Shevchenko A, Bennett BL, Li J, et al. IKK-1 and IKK-2: cytokine-activated I-kappaB kinases essential for NF-kappaB activation. *Science.* 1997;278(5339):860–6. <https://doi.org/10.1126/science.278.5339.860>.
  55. Prusiner SB. Prions. *Proc Natl Acad Sci U S A.* 1998;95(23):13363–83. <https://doi.org/10.1073/pnas.95.23.13363>.
  56. Lim JH, Go G, Lee SH. PrPC regulates the Cancer stem cell properties via interaction with c-met in colorectal Cancer cells. *Anticancer Res.* 2021;41(7):3459–70. <https://doi.org/10.21873/anticancerres.15133>.
  57. Pan Y, Zhao L, Liang J, et al. Cellular prion protein promotes invasion and metastasis of gastric cancer. *FASEB J.* 2006;20(11):1886–8. <https://doi.org/10.1096/fj.06-6138fj>.
  58. Li C, Yu S, Nakamura F, et al. Binding of pro-prion to filamin A disrupts cytoskeleton and correlates with poor prognosis in pancreatic cancer. *J Clin Invest.* 2009;119(9):2725–36. <https://doi.org/10.1172/JCI39542>.
  59. Wenna Ai WR, Diao XL. PRNP gene SYBR green I double standard curve method for fluorescence quantification PCR assay and its preliminary application. *Chinese veterinary. Science.* 2013;43(10):881–6.
  60. Hongwei Y. Pathological observation of MD-infected chickens and quantification of PRNP genes in diseased tissues [D]. Gansu Agricultural University; 2014.
  61. Haq K, Brisbin JT, Thanthrige-Don N, Heidari M, Sharif S. Transcriptome and proteome profiling of host responses to Marek's disease virus in chickens. *Vet Immunol Immunopathol.* 2010;138(4):292–302. <https://doi.org/10.1016/j.vetimm.2010.10.007>.
  62. Isenberg JS, Roberts DD. THBS1 (thrombospondin-1). *Atlas Genet Cytogenet Oncol Haematol.* 2020;24(8):291–9. <https://doi.org/10.4267/2042/70774>.
  63. Sun Y, Shi P, Wu Q, Liu B, Yu Z, Jia H, et al. MiR-222-3p induced by hepatitis B virus promotes the proliferation and inhibits apoptosis in hepatocellular carcinoma by upregulating THBS1. *Hum Cell.* 2021;34(6):1788–99. <https://doi.org/10.1007/s13577-021-00577-1>.
  64. Xu G, Li J, Yu L. miR-19a-3p promotes tumor-relevant behaviors in bladder urothelial carcinoma via targeting THBS1. *Comput Math Methods Med.* 2021;28(2021):2710231. <https://doi.org/10.1155/2021/2710231>.
  65. Diao XL, Wu R, Liu L, et al. Expression patterns of Pr P gene during chicken embryo development. *Asian J Animal Veterinar Adv.* 2012;7(2):199–204.
  66. Denesvre C. Marek's disease virus morphogenesis. *Avian Dis.* 2013;57(2 Suppl):340–50. <https://doi.org/10.1637/10375-091612-Review.1>.
  67. Yan L, Yang Y, Ma X, et al. Effect of two different drug-resistant Staphylococcus aureus strains on the physiological properties of MAC-T cells and their transcriptome analysis. *Front Vet Sci.* 2022;9:818928. <https://doi.org/10.3389/fvets.2022.818928>.

## Publisher's Note

Springer Nature remains neutral with regard to jurisdictional claims in published maps and institutional affiliations.

Ready to submit your research? Choose BMC and benefit from:

- fast, convenient online submission
- thorough peer review by experienced researchers in your field
- rapid publication on acceptance
- support for research data, including large and complex data types
- gold Open Access which fosters wider collaboration and increased citations
- maximum visibility for your research: over 100M website views per year

At BMC, research is always in progress.

Learn more [biomedcentral.com/submissions](https://biomedcentral.com/submissions)

